

## Molecular admixtures and impurities in atmospheric pressure plasma jets

Amanda M. Lietz<sup>1,a)</sup> and Mark J. Kushner<sup>2,b)</sup>

<sup>1</sup>*Department of Nuclear Engineering and Radiological Sciences, University of Michigan, 2355 Bonisteel Blvd., Ann Arbor, Michigan 48109-2104, USA*

<sup>2</sup>*Department of Electrical Engineering and Computer Science, University of Michigan, 1301 Beal Ave., Ann Arbor, Michigan 48109-2122, USA*

(Received 21 July 2018; accepted 27 September 2018; published online 18 October 2018)

A more complete understanding of reactive chemistry generated by atmospheric pressure plasma jets (APPJs) is critical to many emerging medical, agricultural, and water treatment applications. Adding molecular gases to the noble working gas which flows through the jet is a common method to tailor the resulting production of reactive oxygen and nitrogen species (RONS). In this paper, results are discussed from a computational investigation of the consequences of H<sub>2</sub>O and O<sub>2</sub> admixtures on the reactive chemistry of He APPJs flowing into humid air. This investigation, performed with a 2-dimensional plasma hydrodynamics model, addresses the RONS that are initially produced and the evolution of that chemistry on longer time scales. Without an admixture, the impurities in 99.999% pure helium are a major source of RONS. The addition of H<sub>2</sub>O decreases the production of reactive nitrogen species (RNS) and increases the production of reactive oxygen species (ROS). The addition of O<sub>2</sub> significantly decreases the production of RNS, as well as hydrogen-containing ROS, but increases the production of ROS without hydrogen. This selectivity comes from the lower ionization energy of O<sub>2</sub> compared to N<sub>2</sub> and H<sub>2</sub>O, which then allows for charge exchange reactions. These charge exchange reactions change the RONS which are produced in the afterglow by dissociative recombination. The consequences of impurities were also examined. Humid air impurities as low as 10 ppm in the helium can account for 79%-98% of the production of most RONS in the absence of an intentional admixture. The degree to which the impurities affect the RONS production depends on the electrode configuration and can be reduced by molecular admixtures. *Published by AIP Publishing.* <https://doi.org/10.1063/1.5049430>

### I. INTRODUCTION

The reactive chemistry produced in low temperature, atmospheric pressure plasmas has proven beneficial in the fields of plasma medicine, sterilization, and the food supply chain.<sup>1-4</sup> These plasma sources have been shown in some cases to improve wound healing and to selectively kill cancer cells.<sup>5-7</sup> Under the proper conditions, plasma treated seeds grow faster, and plasmas can deactivate fungi on produce and dairy.<sup>4,8</sup> Most of these biological effects are attributed to the production of reactive oxygen and nitrogen species (RONS) which result from dissociation of admixtures or impurities in the initial gas flow or by reaction with the ambient.<sup>9,10</sup> Controlling the fluxes to surfaces of this reactive chemistry is critical to obtaining the desired result in each application. Atmospheric pressure plasma jets (APPJs), which utilize a flowing gas, are a common plasma source for these applications. APPJs generally consist of a dielectric tube through which a rare gas flows with a high voltage electrode (or electrodes) in or wrapped around the tube. APPJs allow more flexibility and control of the plasma chemistry by controlling the gas composition, compared to devices such as dielectric barrier discharges which typically operate in ambient air. These plasma jets, though they appear continuous,

actually operate as a series of pulsed ionization waves, which begin inside the tube and propagate into the plume which mixes with ambient air.<sup>11</sup>

Even a small mole fraction of a molecular gas in a rare gas plasma can significantly affect the electron energy distribution (EED) by introducing inelastic processes with lower threshold energies. For example, the excitation of vibrational and rotational molecular states generally have thresholds on the order of 0.01-0.1 eV. This means that molecular admixtures or impurities, even in small amounts, can change the discharge dynamics, including the electron density and the amount of energy that is coupled into the discharge during a voltage pulse. H<sub>2</sub>O and O<sub>2</sub> are typical admixtures added to APPJ feed-gases with the goal of increasing the generation of particular reactive oxygen species (ROS). Due to the non-linear coupling between the impurities, EEDs, flow dynamics, and mixing with the ambient, the reactive chemistry resulting from the admixtures is not always a straightforward function of concentration.

Several experiments have provided insights into the consequences of admixtures on aspects of the plasma-produced chemistry. In a helium atmospheric pressure glow discharge, Bruggeman *et al.* observed that impurities at concentrations as low as hundreds of ppm dominate the ion chemistry.<sup>12</sup> Increasing the H<sub>2</sub>O concentration in the He decreases the positive ion density and increases the negative ion density, particularly OH<sup>-</sup>(H<sub>2</sub>O)<sub>n</sub>. In laser induced fluorescence (LIF) measurements in an Ar jet, OH densities 1 mm from the jet

<sup>a)</sup>lietz@umich.edu

<sup>b)</sup>Author to whom correspondence should be addressed. mjku@umich.edu

outlet were found to be maximum at 0.5% H<sub>2</sub>O.<sup>13</sup> In a radio frequency (RF) helium APPJ, two photon absorption laser-induced-fluorescence (TALIF) measurements by Knake *et al.* indicated that the O atom density at the jet outlet is a maximum for 0.6% O<sub>2</sub> at constant RF power.<sup>14</sup>

Gas composition in APPJs has been the subject of several modeling studies. Naidis investigated the effects of an air admixture and the humidity of the air in a He APPJ.<sup>15</sup> Increasing the air admixture from 1% to 3% [while increasing the voltage to keep the ionization wave (IW) velocity constant] significantly increased production of O<sub>3</sub> and NO. Increasing the humidity of the air admixture increased the production of OH, decreased the production of O and O<sub>3</sub>, and did not significantly affect NO. Park *et al.* used a global model to study admixtures of O<sub>2</sub> in He and Ar atmospheric pressure glow discharges.<sup>16</sup> At 1% O<sub>2</sub>, most of the electron energy losses were by collisions with O<sub>2</sub>. At constant power, adding O<sub>2</sub> decreased the electron density ( $n_e$ ), and increased the production of O and O<sub>3</sub>, with the effects being most dramatic in the first 1% of O<sub>2</sub> added. Schröter *et al.* used a global model to study a humid He radio-frequency APPJ, showing a decrease in the electron density and an increase in nearly all reactive oxygen species with an increase in the H<sub>2</sub>O admixture.<sup>17</sup>

Admixtures have also been shown to change the biological outcomes in applications of APPJs. In experiments by Joh *et al.*, an O<sub>2</sub> admixture in a helium APPJ increased plasma-induced apoptosis in cancer cells.<sup>18</sup> Humidified He and humidified He/O<sub>2</sub> have been less effective than dry He/O<sub>2</sub> at inducing apoptosis.<sup>6</sup> Lin *et al.* have shown that an O<sub>2</sub> admixture of 0.02% in an Ar plasma jet is most effective for deactivating bacterial endospores.<sup>1</sup>

In this paper, we report on a 2-dimensional computational investigation of the effects of O<sub>2</sub> and H<sub>2</sub>O admixtures in He APPJs having *as delivered impurities* on IW propagation and the initial production of RONS. The amounts of RONS that flow out of the computational domain are compared as a measure of the maximum reactivity available for surface processing. These products are generated after allowing several ms for initially produced radicals to react with each other and the admixture, mix with the surrounding air, and flow downstream. The energy normalized RONS production was also compared to distinguish the role of the changes in energy coupled to the plasma as the admixture is varied from changes in the gas composition. The model is described in Sec. II. The discussion of results in Sec. III includes a brief overview of the base case in Part A, the consequences of H<sub>2</sub>O admixtures in Part B and O<sub>2</sub> admixtures in Part C, and the role of impurities in Part D. Concluding remarks are in Sec. IV.

## II. DESCRIPTION OF THE MODEL

The model used in this investigation, *nonPDPSIM*, is a 2-dimensional plasma hydrodynamics simulation that is described in detail by Norberg *et al.*<sup>19</sup> *nonPDPSIM* solves Poisson's equation on an unstructured mesh and contains modules for neutral chemistry, fluid mechanics, and radiation transport. The model uses time slicing algorithms which

enable Poisson's equation and charged species transport to be solved with a time scale of several picoseconds during the voltage pulse, while the fluid dynamics are updated on nano-second time scales. Electron impact rate coefficients are obtained from solutions of Boltzmann's equation for electron energy distributions using a two-term spherical harmonic approximation. The reaction mechanism contains 51 species addressing helium and humid air – 16 charged species, 35 neutral species. The mechanism contains 753 reactions, including 175 electron impact reactions. The reaction mechanism is discussed by Norberg *et al.* and therefore will only be summarized here.<sup>19,20</sup> (Note that in Ref. 20, species having the same rate coefficient for a reaction are grouped into a single entry. For example, a Penning ionization reaction having the same rate coefficient for all excited states of He is represented by the species He\*.)

The mechanism treats the lower energy levels of electronically excited helium explicitly [He(2<sup>3</sup>S), He(2<sup>1</sup>S), He(2<sup>3</sup>P), He(2<sup>1</sup>P)], while the more highly excited states are lumped into He(3P) and He(3S). The He excimers are lumped into a single excimer state (He<sub>2</sub>\*), which is not radiatively trapped. The primary ions, which are generated by electron impact on the flowing gases, are He<sup>+</sup>, N<sub>2</sub><sup>+</sup>, O<sub>2</sub><sup>+</sup>, O<sub>2</sub><sup>-</sup>, and H<sub>2</sub>O<sup>+</sup>. For these conditions, He<sup>+</sup> is dominantly produced by direct electron impact ionization of ground state He, and to a lesser extent by stepwise ionization and Penning ionization (He\* + He\* → He + He<sup>+</sup> + e, where He\* includes all electronically excited states of He). Although the rate coefficient for electron impact ionization of excited states greatly exceeds that for He, the mole fraction of the excited states is also small, resulting in the stepwise process not dominating ionization. N<sub>2</sub><sup>+</sup>, O<sub>2</sub><sup>+</sup>, and H<sub>2</sub>O<sup>+</sup> are produced by electron impact ionization, Penning ionization, and charge exchange. O<sub>2</sub><sup>-</sup> is a result of 3-body electron attachment to O<sub>2</sub>. Dissociative electron impact ionization or dissociative attachment produces N<sup>+</sup>, O<sup>+</sup>, O<sup>-</sup>, H<sup>+</sup>, and OH<sup>-</sup>. The reaction mechanism contains a limited number of higher order and cluster ions including N<sub>4</sub><sup>+</sup>, H<sub>3</sub>O<sup>+</sup>, and H<sub>3</sub>O<sup>+</sup>(H<sub>2</sub>O). In the presence of water vapor, more and larger water cluster ions would actually form; however, these have not been included due to the additional computational cost. These water-cluster ions may have some effect on the recombination rates, but the neutral RONS produced as a result of recombination and ion-ion neutralization reactions are typically unaffected by the surrounding water molecules.<sup>21</sup>

The electronically excited states associated with humid air are N<sub>2</sub>\* [a lumped state including N<sub>2</sub>(A<sup>3</sup>Σ), N<sub>2</sub>(B<sup>3</sup>Π), N<sub>2</sub>(W<sup>3</sup>Δ), N<sub>2</sub>(B<sup>3</sup>Σ), N<sub>2</sub>(a<sup>1</sup>Σ), N<sub>2</sub>(ã<sup>1</sup>Π), N<sub>2</sub>(w<sup>1</sup>Δ)], and N<sub>2</sub>\*\* [N<sub>2</sub>(C<sup>3</sup>Π) and N<sub>2</sub>(E<sup>3</sup>Σ)]. Excited states of oxygen include O<sub>2</sub>\* referring to O<sub>2</sub>(<sup>1</sup>Δ) and O<sub>2</sub>\*\* referring to O<sub>2</sub>(b<sup>1</sup>Σ<sub>g</sub>). O\* [O(2<sup>1</sup>D) and O(2<sup>1</sup>S)] and N\* [N(2<sup>2</sup>D) and N(2<sup>2</sup>P)] are included as a result of dissociation of O<sub>2</sub> and N<sub>2</sub>. N<sub>2</sub>(v) is the only vibrationally excited state that is explicitly tracked in the mechanism. All other vibrational and rotational collisions are accounted for in the electron energy losses and the gas heating, but the density of the vibrationally and rotationally excited products are not calculated.

The main species of interest in the biological applications are RONS, which can have longer lifetimes allowing

them to reach a biological sample. Reactive oxygen species include  $O$ , which forms by dissociation of  $O_2$ , and then reacts with  $O_2$  to form  $O_3$ . The dissociation of  $H_2O$  leads to the production of  $H$  and  $OH$ .  $H$  then either reacts with itself to form  $H_2$  or reacts with  $O_2$ , generating  $HO_2$ .  $OH$  reacts with itself to form  $H_2O_2$ . The reactive nitrogen species generally begin with the conversion of  $N^*$  reacting with  $O_2$  to form  $NO$ . Once  $NO$  forms, it can remain in that form or react with other ROS and reactive nitrogen species (RNS) producing various  $N_xO_y$  (including  $NO_2$ ,  $NO_3$ ,  $N_2O_3$ ,  $N_2O_4$ , and  $N_2O_5$ ). Many of these  $N_xO_y$  species react with  $H_2O$  or  $OH$  producing  $HNO_x$  (including  $HNO_2$ ,  $HNO_3$ , and  $ONOOH$ ).

The geometry and flow conditions of the APPJ of this study are shown in Fig. 1(a). The APPJ is a dielectric tube (relative permittivity,  $\epsilon_r = 4$ ) with an inner diameter of 1 mm and an outer diameter of 1.5 mm. A powered ring electrode 1 mm wide is located 8 mm from the end of the tube and is covered with a thin shielding dielectric. The entire computational domain, using cylindrical symmetry, is 2.95 cm by 6.44 cm. The electrical ground is at the pump face, located 1.55 cm from the end of the tube and at a radius of 1.4 cm.

The fluid module for neutral gas flow was initially run for 12 ms, which was sufficient for the fluid dynamics to reach a steady state, before the voltage pulse was applied. He containing impurities of  $O_2/N_2/H_2O = 2.4/2.9/4.7$  ppm flowed through the tube at 2 slm. This choice of impurities was based on specifications from Matheson Tri-gas Inc. and Linde Group Inc. for 99.999% pure He. In the cases of an admixture, the total mass flow rate remained at 2 slm, and only the composition of the gas changed. Humid air flowed into the domain through the annular area around the tube at 4 slm. This humid air flow represents the air entrainment by the helium which would occur in an open air environment and which is not captured in this limited computational domain. A pressure boundary condition of 1 atm was applied at the pump surface. The steady state axial fluid speed is shown in Fig. 1(b).

The simplified radiation transport model included photoionization of  $N_2$ ,  $O_2$ , and  $H_2O$  by  $He_2^*$ , which is a lumped state of all He excimers. The plasma was initialized with a small cloud of electrons 1.4 mm in diameter at the height of the powered electrode having a peak density of  $10^{11} \text{ cm}^{-3}$ . A  $-10 \text{ kV}$  pulse with a 20 ns rise time was applied to the powered electrode. The applied voltage remained at  $-10 \text{ kV}$  for 130 ns, followed by a 20 ns voltage fall time, bringing the total voltage-on period to 170 ns. Poisson's equation was solved for 30 ns after the voltage returned to 0 kV (200 ns total). After this time, the plasma was assumed to be charge neutral, Poisson's equation was no longer solved, and the electron temperature ( $T_e$ ) was fixed at 0.025 eV. Transport and chemistry of charged and neutral species were addressed while enforcing charge neutrality for the remainder of the simulation (16 ms total) as the RONS flowed out of the computational domain at the pump. The times that are required for each fluid element to reach the pump surface are shown in Fig. 1(b), which indicate that all of the RONS have exited the domain by the end of the simulation. Results will be discussed for a single voltage pulse for each condition, which

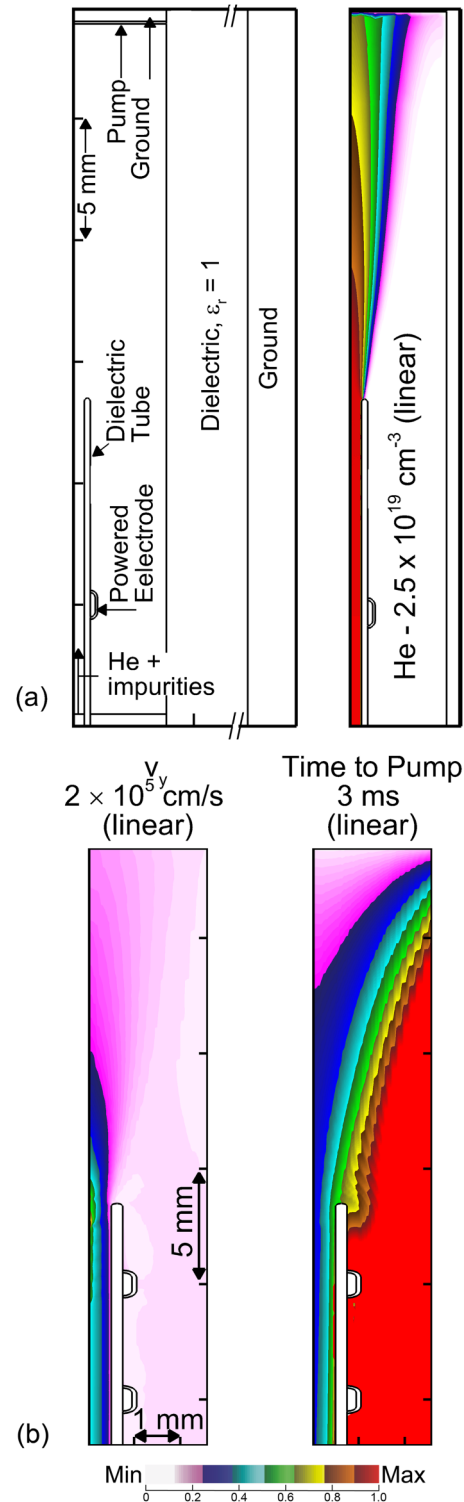


FIG. 1. Computational geometry and flow dynamics for the base case simulations. (a) (left) Geometry and (right) steady state He density. The dielectric tube has a 1 mm inner diameter. (b) (left) Axial component of the fluid velocity and (right) time to reach the pump from each point in the computational domain. Note that in (b) the aspect ratio has been modified to show detail inside the tube.

limits the direct applicability of these results to repetition rates of hundreds of Hz to perhaps a few kHz. Significantly higher repetition rates would result in there being significant mixing between reactants produced on previous pulses with those produced during the current pulse.

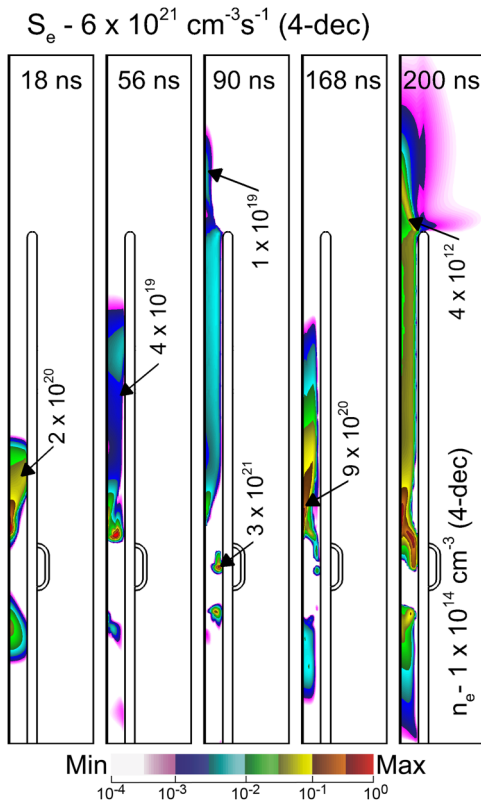


FIG. 2. Ionization wave propagation in the base case atmospheric pressure plasma jet.  $S_e$  is the electron impact ionization source term, shown in the left four frames. The electron density,  $n_e$ , at the end of the voltage pulse is in the rightmost frame. The values are plotted on a 4-decade log scale with the maxima indicated in the figure.

Computational diagnostics were used to characterize RONS production. The first is the *inventory* of species in the computational domain, which is the volume integral of densities. The second, more appropriate to gauge treatment of surfaces, is the number of atoms or molecules of a species flowing out of the computational domain at the pump face. This *total fluence* is the time integral of the fluxes at each point of the pump-face, which is then integrated over the area of the pump face. Diagnostics intended to measure the efficiency of production were also used. The *specific inventory* is the inventory divided by the energy deposition during the pulse. The *specific total fluence* is the total fluence divided by the energy deposition during the pulse.

### III. RONS PRODUCTION FOR HE APPJS WITH ADMIXTURES AND IMPURITIES

#### A. Base case

An overview of the ionization wave dynamics of the jet appears in Fig. 2. When the voltage is applied, the plasma propagates as an ionization wave (IW) beginning at the powered electrode. While propagating inside the tube, the IW intensity has a maximum at the surface of the tube, making the IW annular in shape. Upon exiting the tube, the IW follows the interface between the helium and humid air, where many of the RONS are generated. The behavior of the IW and RONS production in this APPJ with a single ring

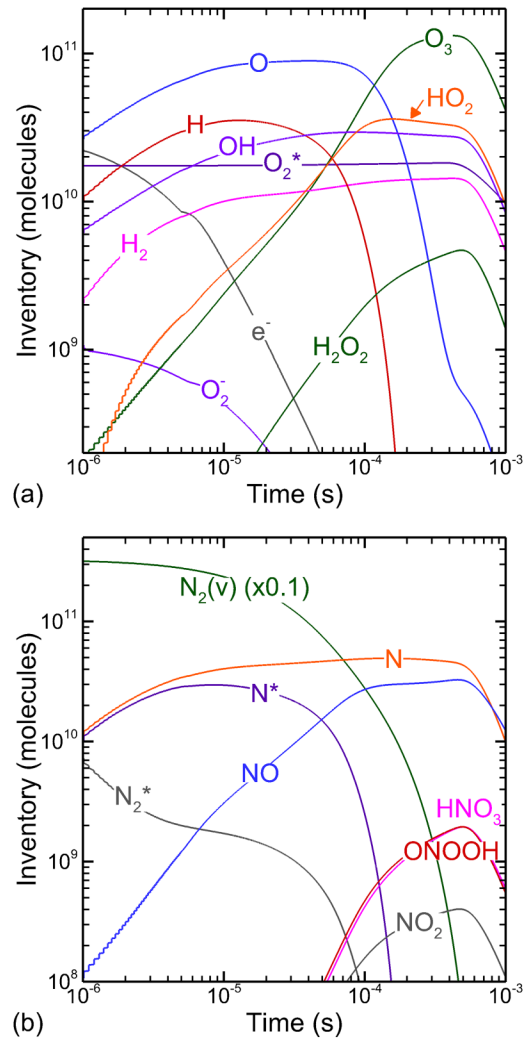


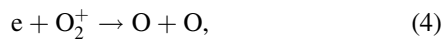
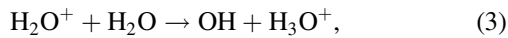
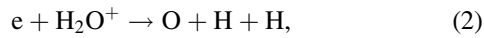
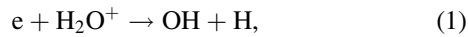
FIG. 3. The inventory (volume integrated number density) of reactive species as a function of time after the start of the voltage pulse. At  $400 \mu\text{s}$ , reactive species reach the pump and begin exiting the computational domain. The plots have been smoothed. (a) Species which do not contain nitrogen. (b) Species which contain nitrogen.

electrode was discussed in Ref. 22, and the analysis will not be repeated here.

The inventories in the entire computational domain are shown as a function of time after the discharge pulse in Fig. 3 and demonstrate the conversion of the initially generated reactivity to more complex and stable species. At approximately  $400 \mu\text{s}$ , the cloud of RONS first generated by the plasma comes into contact with the pump, and the species inventories decrease as these species exit the computational domain. Some RONS present before  $1 \mu\text{s}$  are a direct result of electron impact processes by the IW. For example,  $\text{N}_2^*$  and  $\text{N}_2(v)$  are a result of electron impact excitation of  $\text{N}_2$ .  $\text{O}_2^-$  forms through three body electron attachment on  $\text{O}_2$ , and  $\text{O}_2^*$  is generated by electron impact excitation of  $\text{O}_2$ .

One feature of the inventories in Fig. 3 is that many of the dissociation products, such as O, N,  $\text{N}^*$ , OH, and H, trace much of their production to the afterglow. The plasma-on period is  $200 \text{ ns}$ , after which the electron temperature was fixed to  $0.025 \text{ eV}$ , resulting in most inelastic electron impact processes having a negligible rate. However, the

dissociation producing these species occurred between 1 and 10  $\mu\text{s}$ . The production of these species is the result of a cascade of charge exchange and electron-ion recombination reactions that occur after the plasma pulse terminates, including



These reactions are the primary source of OH, H, O, N, and  $\text{N}^*$  in the base case. The  $\text{H}_2\text{O}^+$ ,  $\text{O}_2^+$ , and  $\text{N}_2^+$  form by electron impact ionization, charge exchange reactions, and Penning ionization. O produced inside the tube dominantly results from dissociative recombination of  $\text{O}_2^+$  [Eq. (4)]. O is also produced outside of the tube by dissociative excitation transfer,  $\text{N}_2^* + \text{O}_2 \rightarrow \text{N}_2 + \text{O} + \text{O}$ , where  $\text{N}_2^*$  is dominated by  $\text{N}_2(\text{A}^3\Sigma)$ .

On time scales of 100  $\mu\text{s}$ , these initially produced species react with other RONS and with the surrounding humid air. O atoms, with an inventory as high as  $9 \times 10^{10}$  atoms, are nearly completely converted to  $\text{O}_3$ , which reaches inventories as high as  $1 \times 10^{11}$  molecules. H reacts with  $\text{O}_2$  to form  $\text{HO}_2$  as it flows out of the tube and contacts the air. To a lesser degree, some of the H recombines to form  $\text{H}_2$ . OH reacts to form  $5 \times 10^9$  molecules of  $\text{H}_2\text{O}_2$ , but this occurs slowly enough that much of the OH ( $3 \times 10^{10}$  molecules) flows out of the domain. NO primarily forms by  $\text{N}^* + \text{O}_2 \rightarrow \text{NO} + \text{O}^*$ , a reaction which occurs when the  $\text{N}^*$ , formed inside of the tube, flows out of the tube and contacts air.  $\text{NO}_2$  production primarily comes from  $\text{NO} + \text{HO}_2 \rightarrow \text{NO}_2 + \text{OH}$  and  $\text{NO} + \text{O} + \text{M} \rightarrow \text{NO}_2 + \text{M}$ . Some of these RONS react through several pathways to convert NO or  $\text{NO}_2$  into  $\text{HNO}_2$ ,  $\text{HNO}_3$ , and  $\text{ONOOH}$ . Only a fraction of the NO (with an inventory of  $3 \times 10^{10}$  molecules) is converted to  $\text{HNO}_x$ , which remains below  $4 \times 10^9$  molecules.

The times required for RONS to transit to the pump from each point in the computational domain are shown in Fig. 1(b). These values were calculated by integrating  $v^{-1}$ , where  $v$  is the fluid velocity, along a streamline to the pump surface. Reactants produced on-axis near the powered electrode take 0.75 ms to reach the pump, while species produced at  $r = 250 \mu\text{m}$  near the powered electrode require 1.1 ms to reach the pump. Species produced in the shear layer just outside of the tube take 1.7 ms to reach the pump. Viscosity results in the peak velocity being on-axis, resulting in a longer transit time to the pump at larger radii. By 2 ms after the plasma pulse, most of the RONS have reached the pump surface.

The spatially integrated fluxes of plasma produced species integrated over the area of the pump surface as a function of time, normalized to each individual maximum

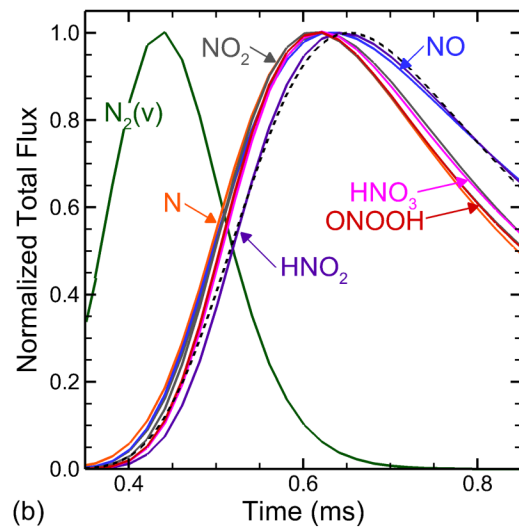
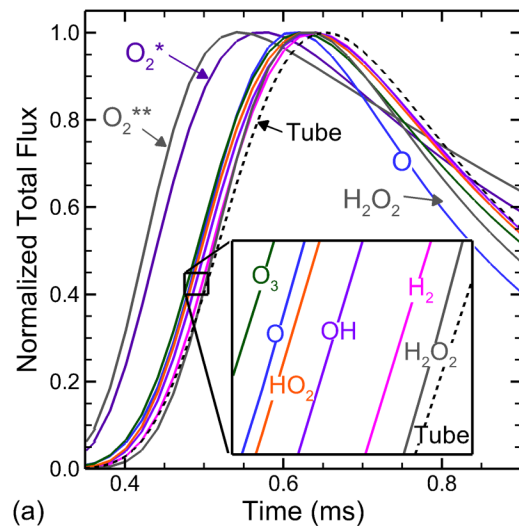


FIG. 4. The flux of plasma produced species at the pump as a function of time in the base case. The values are normalized to the maximum flux for each species. There is a delay following the voltage pulse before a significant flux arrives at the pump, which indicates the location of production based in Fig. 1(b). The dashed line is the resultant flux from the simple case of an unreactive species generated uniformly within the tube. (a) ROS and (b) RNS.

flux, are shown in Fig. 4. Had the initial reactive species been produced as a delta-function in space and time, and the gas flow had a uniform speed, the reactants would arrive as a delta-function at the pump face. The dashed line in Fig. 4 represents the theoretical flux of an inert species generated uniformly inside the tube in the steady state flow field and simulating the advection and diffusion of this species as the plume flows toward the pump. The flux of this species rises sharply at 0.45 ms, when it first reaches the surface and decreases over the next 2 ms as the species which have diffused away from the axis continue to arrive at the surface. The time dependencies of the total fluxes result from several effects. Due to the spatial dynamics of the IW, reactivity is produced with a distribution of axial and radial locations. Even with a constant gas speed, reactants from these different

locations would arrive at the pump face with a distribution of time delays. Due to viscous forces, the axial flow speed is also a function of position. Species produced at the edge of the plume will be entrained in the slower shroud flow of air and arrive at the pump face considerably later.  $O_2^*$ ,  $O_2^{**}$ , and  $N_2(v)$  were primarily produced outside of the tube closer to the pump and therefore reach the pump earlier and have an earlier increase in their fluxes. The fluxes of most species increase more rapidly earlier in time than the ideal case, because there is some production of these species outside of the tube closer to the pump. These rise times indicate that  $O_3$  and  $HO_2$  production is largely close to the axis and at greater heights, while species such as  $H_2$  and  $H_2O_2$  trace their origins to larger radii deeper inside the tube.

## B. Water admixture

Water vapor is typically added to the feedstock gas with the goal of increasing the production of hydrogen-containing species such as OH and  $H_2O_2$ . The admixture of  $H_2O$  to the He flow discussed in this section is in addition to the impurities that are in the base case ( $O_2/N_2/H_2O = 2.4/2.9/4.7$  ppm). The helium mole fraction was reduced when having an admixture so that the total flow rate through the tube remained constant at 2 slm. The admixture values are referred to in percent number density (i.e., mole fraction). As the  $H_2O$  admixture increased from 2.9 ppm to 0.7% (7000 ppm), the IW speed increased, exiting the tube 46 ns earlier compared to the base case. The electron impact ionization rate in the IW increased with increasing admixture from  $3 \times 10^{19}$  to  $7 \times 10^{20} \text{ cm}^{-3} \text{ s}^{-1}$ . The maximum electron density outside of the tube at  $t = 200$  ns increased from  $8 \times 10^{12}$  to  $4 \times 10^{13} \text{ cm}^{-3}$ . The total energy deposited in the plasma as a function of the  $H_2O$  mole fraction is shown in Fig. 5(a) and increased from  $14.7 \mu\text{J}$  to  $135 \mu\text{J}$  as the  $H_2O$  admixture increased from 2.4 ppm to 0.7%. With higher admixtures,  $T_e$  was slightly lower in the IW front (5.7 vs. 5.2 eV), and  $T_e$  thermalized more quickly after the IW passed. The more rapid electron thermalization is due to the more rapid electron energy losses provided by low threshold inelastic collisions with  $H_2O$ , such as vibrational excitation.

Penning ionization increases with  $H_2O$  admixture, resulting in higher electron density, higher conductivity, and higher energy deposition for a given voltage. Direct electron impact ionization of  $H_2O$  also occurs, but this process is not the primary source of electrons. In the base case, the rate coefficient for electron impact ionization of helium is about 3 orders of magnitude smaller than that of  $H_2O$ . However, the density of He is 5 orders of magnitude larger, resulting in direct electron impact ionization of He dominating over that of  $H_2O$ . Penning ionization of  $H_2O$  by He excited states becomes the primary source of electrons for admixtures above 0.02%. At 0.5%  $H_2O$ , the number of electrons generated by Penning ionization of  $H_2O$  is approximately 10 times greater than those generated by electron impact ionization reactions. The plasma more rapidly recombined when containing higher mole fractions of  $H_2O$  by recombination of electrons with  $H_3O^+(H_2O)$ . In the base case, the electron density decreased by an order of magnitude after about  $12 \mu\text{s}$ . In the 0.7%  $H_2O$  case, this decrease in electron density occurred in  $1 \mu\text{s}$ .

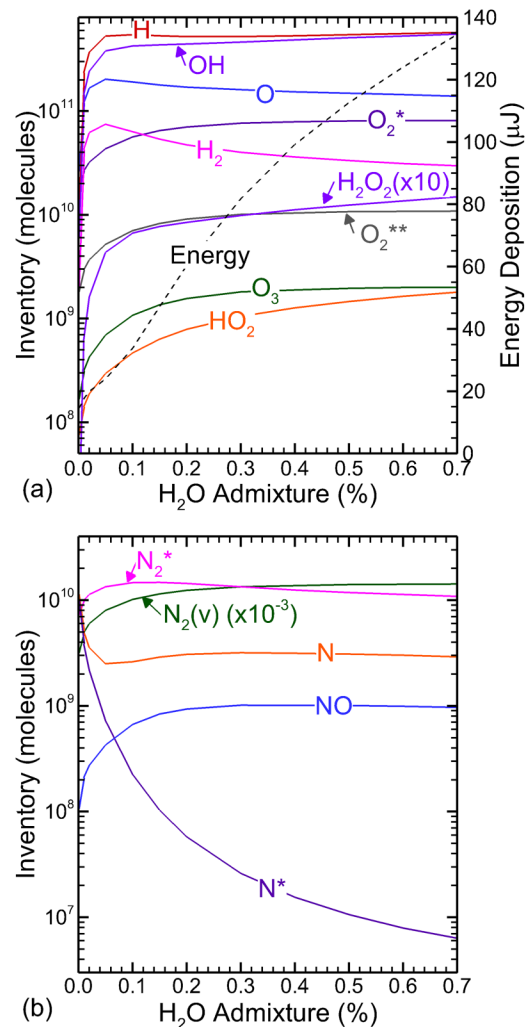


FIG. 5. The inventories of RONS at  $1 \mu\text{s}$  after the start of the voltage pulse as a function of  $H_2O$  admixture in the He flow. (a) ROS and (b) RNS.

The volume integrated number densities, the inventories, of various RONS are shown in Fig. 5. These are the inventories  $1 \mu\text{s}$  after the start of the voltage pulse, which largely reflect the initial RONS production. At this time, most of the initial ions have reacted or recombined; however, the fluid motion has not convected species produced in the tube into the ambient. Most of the initially produced RONS increased with  $H_2O$  density, in part because the energy deposition, electron density, and IW propagation outside the tube increased with increasing  $H_2O$  admixture. The exceptions to this behavior are N and  $N^*$ , which decreased with  $H_2O$  admixture, and  $N_2^*$ ,  $H_2$ , and O, whose inventories were maximum at 0.05%  $H_2O$ . In the base case and at low admixtures, most of the N and  $N^*$  was generated in the afterglow, between 200 ns and  $3 \mu\text{s}$  by dissociative recombination,  $e + N_2^+ \rightarrow N + N^*$ . This process resulted in N and  $N^*$  inventories as high as  $1 \times 10^{10}$  atoms at  $1 \mu\text{s}$ . As the  $H_2O$  admixture increased,  $N_2^+$  charge exchanged with  $H_2O$  to produce  $H_2O^+$ , resulting in little production of N or  $N^*$  in the afterglow. In this case, most of the N was produced by electron impact dissociation of  $N_2$  during the voltage pulse. As the electron density and IW intensity increased with  $H_2O$  admixture,  $N_2^*$  production by electron

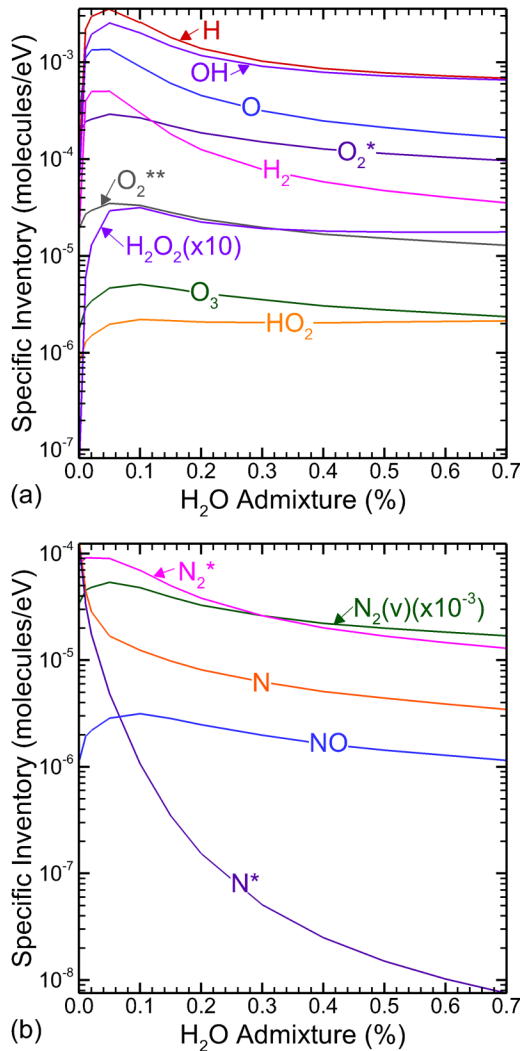


FIG. 6. The inventories of RONS at  $1 \mu\text{s}$  after the start of the voltage pulse per eV of energy deposition in the plasma (the specific inventory) as a function of H<sub>2</sub>O admixture in the He flow. (a) ROS and (b) RNS.

impact reactions initially increased its inventory up to  $1.5 \times 10^{10}$  molecules. As the H<sub>2</sub>O admixture increased above 0.1%, the depletion of high energy electrons by inelastic collisions with H<sub>2</sub>O decreased the rate of electron impact excitation of N<sub>2</sub>. Much of the O in the base case was formed between 200 ns and  $3 \mu\text{s}$  after the voltage pulse by  $e + \text{O}_2^+ \rightarrow \text{O} + \text{O}$  and  $\text{N}_2^* + \text{O}_2 \rightarrow \text{N}_2 + \text{O} + \text{O}$ . As the H<sub>2</sub>O admixture increases, the dissociative recombination reaction  $e + \text{H}_2\text{O}^+ \rightarrow \text{H} + \text{H} + \text{O}$  dominates the production of O inside the tube. As the admixture continues to increase above 0.1%, the H<sub>2</sub>O<sup>+</sup> ions begin to react with H<sub>2</sub>O ( $\text{H}_2\text{O}^+ + \text{H}_2\text{O} \rightarrow \text{H}_3\text{O}^+ + \text{OH}$ ) instead of recombining with electrons, and less O is formed. Therefore, at higher admixtures, O is predominantly produced outside the tube by reactions of N<sub>2</sub><sup>\*</sup> with O<sub>2</sub>.

H<sub>2</sub> is largely produced by recombination of H atoms. However, for a density of H of  $10^{14} \text{ cm}^{-3}$ , this conversion occurs in hundreds of ms and so would not significantly affect the inventory at  $1 \mu\text{s}$ . Wall recombination of H was the dominant source of H<sub>2</sub> at  $1 \mu\text{s}$ , though several electron impact and recombination processes also generate H<sub>2</sub>. The

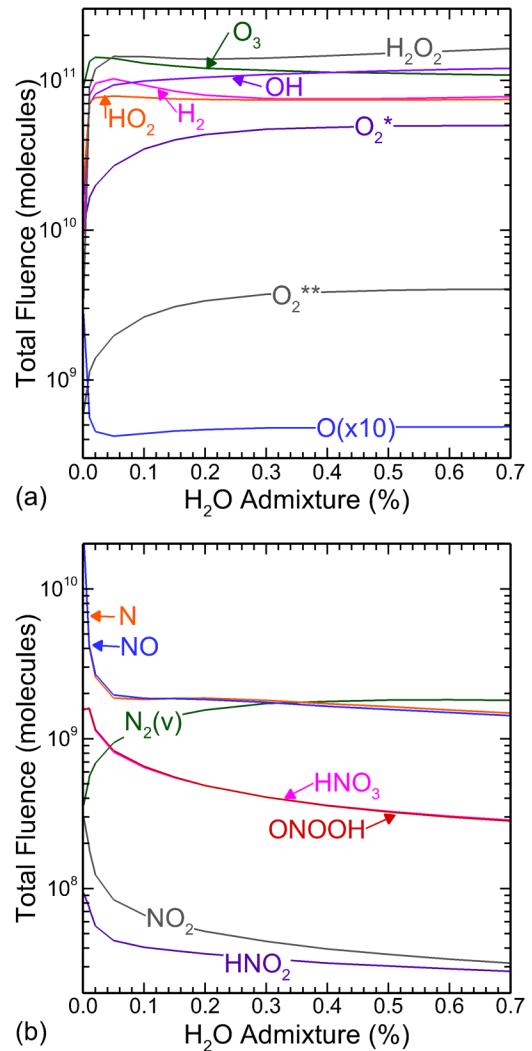


FIG. 7. The total fluence of RONS crossing the pump as a function of H<sub>2</sub>O admixture in the He flow. The fluence was integrated across the area of the pump surface which yields the total number of molecules exiting the computational domain. (a) ROS and (b) RNS.

importance of wall recombination reactions in humid He plasma chemistry was investigated by Schröter *et al.*<sup>17</sup> As the H<sub>2</sub>O admixture increased beyond 0.1%, the H was selectively generated outside of the tube by the more deeply penetrating IW, where it rapidly reacted with O<sub>2</sub> to form HO<sub>2</sub>.

The largest change in densities of species occurred in the first 0.1% of addition of H<sub>2</sub>O. OH, H, and H<sub>2</sub>O<sub>2</sub> inventories were the most sensitive, all increasing by nearly 2 orders of magnitude from the initial mixture to 0.1%. These species require water in their formation and particularly benefit from dissociative recombination of H<sub>2</sub>O<sup>+</sup> producing either the species themselves or their precursors. The inventories of these species were increased not only by the increased mole fraction of H<sub>2</sub>O, but also by the increased energy deposition and plasma densities.

The inventories of species  $1 \mu\text{s}$  after the start of the voltage pulse divided by the energy deposition in the plasma, referred to as the *specific inventories*, are shown in Fig. 6. The specific inventory of H reaches  $4 \times 10^{-3}$  atoms/eV, while the specific inventory of NO does not exceed  $3 \times 10^{-6}$

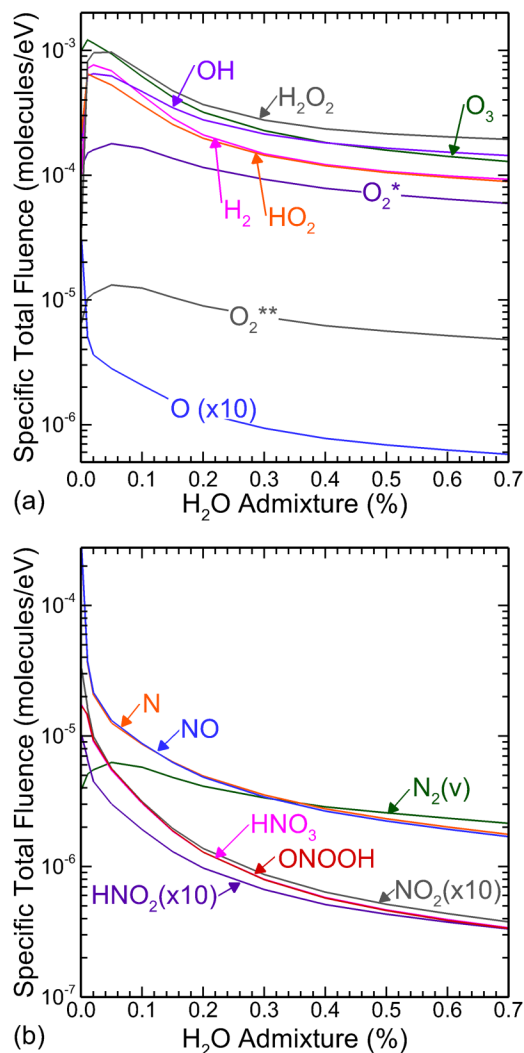


FIG. 8. The total fluence of RONS across the pump surface per eV of energy deposition in the plasma (the specific total fluence) as a function of H<sub>2</sub>O admixture to the He flow. (a) ROS and (b) RNS.

molecules/eV. As the first 0.05% of H<sub>2</sub>O was added, the energy efficiency of the production of all RONS, except N and N<sup>\*</sup>, increased. Therefore, for the first 0.05% of H<sub>2</sub>O, the increase in most species was not solely due to the increase in energy deposition. As H<sub>2</sub>O is added, discharge power is preferentially channeled into H<sub>2</sub>O, thereby initially producing larger densities of H and OH leading to a greater specific inventory of H<sub>2</sub>, H<sub>2</sub>O<sub>2</sub>, and HO<sub>2</sub>. The IW also propagates more quickly as the admixture is increased to 0.05%, with a speed of  $1.2 \times 10^7$  cm/s compared to  $8 \times 10^6$  cm/s in the base case. As the IW exits the tube earlier in the pulse, the fraction of energy deposited outside the tube increases from 5.7% to 9.3%. The species which require the excitation of O<sub>2</sub> (O<sub>2</sub><sup>\*</sup> and O<sub>2</sub><sup>\*\*</sup>) and some species which are a result of dissociation or excitation of N<sub>2</sub> [N<sub>2</sub><sup>\*</sup>, NO, N<sub>2</sub>(v)] also have specific inventories which increased as H<sub>2</sub>O admixture was increased up to 0.05%. These species are dominantly produced outside of the tube at these time scales, especially at low admixture concentration.

As the H<sub>2</sub>O admixture increases from the base case to 0.05%, the dominant mechanism of O generation is e +

H<sub>2</sub>O<sup>+</sup> → H + H + O inside the tube, and therefore, the specific inventory of O shows the same trends as that of H. At larger admixtures, hydronium production occurs more rapidly than electron ion recombination, and the trend of O specific inventory is more consistent with that of N<sub>2</sub><sup>\*</sup> producing O by dissociative excitation transfer to O<sub>2</sub>.

Increasing the H<sub>2</sub>O mole fraction above 0.1% increased the total energy deposition from 34 to 135 μJ, while resulting in diminishing incremental RONS production and decreasing specific inventory for nearly all species. The HO<sub>2</sub>, however, has a specific inventory which continues to increase slightly with the H<sub>2</sub>O admixture. This additional production of HO<sub>2</sub> results from the increase in IW speed, further penetration of the IW into the ambient, and increase in the H produced outside of the tube, where it is more quickly converted to HO<sub>2</sub> due to the higher local O<sub>2</sub> density.

The total number of atoms or molecules of each species that exit the computational domain are shown in Fig. 7. These values, referred to as the *total fluence*, are the flux across the pump surface integrated in space and time. These fluences result from the initial reactive species shown in Fig. 5 after they were processed by mixing and reacting with the surrounding humid air and other RONS. The fluences of H<sub>2</sub>O<sub>2</sub>, HO<sub>2</sub>, and O<sub>3</sub> directly follow the trends of their precursors at 1 μs—OH being the precursor for H<sub>2</sub>O<sub>2</sub>, H for HO<sub>2</sub>, and O for O<sub>3</sub>. The H<sub>2</sub>O<sub>2</sub> and HO<sub>2</sub> total fluences are nearly unchanging above 0.05% H<sub>2</sub>O, as were the OH and H inventories at 1 μs. The O<sub>3</sub> total fluence is maximum at 0.02% H<sub>2</sub>O, and slowly decreasing with additional admixture, as is the case for O inventories. OH, H<sub>2</sub>, N, O<sub>2</sub><sup>\*</sup>, O<sub>2</sub><sup>\*\*</sup>, and N<sub>2</sub>(v) follow the same trends with admixture as their inventories at 1 μs, though their absolute densities change significantly between 1 μs and when they exit at the pump. Most of these species inventories decrease by a factor of 2–4 from their values at 1 μs while flowing to the pump as they undergo reactions or collisional quenching. The inventory of N<sub>2</sub>(v) decreases more significantly, by a factor of 10<sup>4</sup>, due to collisional quenching. The inventory of H<sub>2</sub> increases by 25% as H atoms recombine on longer time scales.

The fluences of reactive nitrogen species (RNS) all significantly decreased with increasing H<sub>2</sub>O admixture. The inventory of N<sup>\*</sup> decreases with H<sub>2</sub>O admixture (shown in Fig. 5), while N<sup>\*</sup> is the primary precursor to rapidly forming NO at room temperature. The total fluence of NO decreases from  $2 \times 10^{10}$  to  $1 \times 10^9$  molecules as the H<sub>2</sub>O admixture increases. NO formation is the first step required to form most of the other RNS—NO<sub>2</sub>, HNO<sub>2</sub>, HNO<sub>3</sub>, and ONOOH—and so their fluences also decrease.

The total fluences integrated at the pump divided by the total energy deposited in the plasma, referred to as the *specific total fluences*, as a function of H<sub>2</sub>O admixture are shown in Fig. 8. The trends for specific total fluence as a function of H<sub>2</sub>O admixture generally reflect the specific inventories of their precursors (shown in Fig. 6). The specific total fluences of H<sub>2</sub>O<sub>2</sub>, HO<sub>2</sub>, and O<sub>3</sub> were within a factor of 5 of the specific inventories of their precursors at 1 μs and follow the same trends. OH, N, O<sub>2</sub><sup>\*</sup>, O<sub>2</sub><sup>\*\*</sup>, and N<sub>2</sub>(v) followed the same trends as at 1 μs, though the magnitudes are reduced due to reactions or collisional

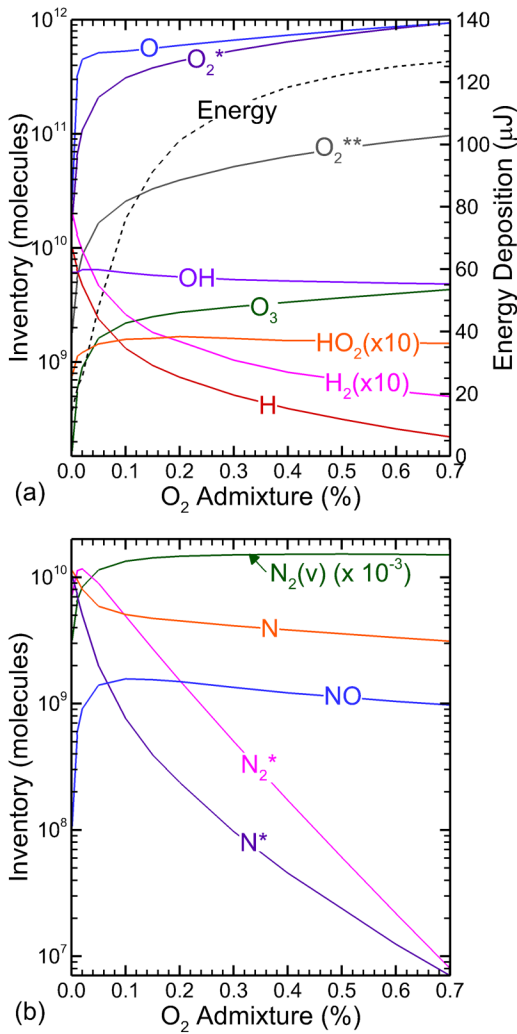


FIG. 9. The inventory of RONS  $1\ \mu\text{s}$  after the start of the voltage pulse as a function of  $\text{O}_2$  admixture to the He flow. (a) ROS and (b) RNS. The energy deposited in the plasma is also plotted in (a).

quenching. The  $\text{H}_2$  specific total fluence follows the same trends as its specific inventory at  $1\ \mu\text{s}$  but is larger as H continues to recombine.

The species whose production requires the dissociation of  $\text{N}_2$  (N, NO,  $\text{NO}_2$ , and  $\text{HNO}_x$ ) all had specific total fluences which decreased monotonically by 2 orders of magnitude with increasing  $\text{H}_2\text{O}$  admixture. The specific total fluences of N and NO decreased from  $3 \times 10^{-4}$  to  $2 \times 10^{-6}$  molecules/eV, while that of  $\text{HNO}_3$  decreased from  $2 \times 10^{-5}$  to  $3 \times 10^{-7}$ . The specific RNS production decreased monotonically as the  $\text{H}_2\text{O}$  fraction increased, in spite of the fraction of energy deposited outside of the tube having a maximum at 0.05%  $\text{H}_2\text{O}$ . Even when the IW propagation (and energy deposition) outside of the tube increases, production of  $\text{N}^*$  inside the tube is still the main source of RNS production.

As the  $\text{H}_2\text{O}$  admixture is increased from 0.1% to 0.7%, the energy deposition in the plasma increases from  $34$  to  $135\ \mu\text{J}$ ; however, the production of most RONS changes little. Although the energy deposited outside the tube nearly doubles, the fraction of energy deposited outside the tube decreases from 8.7% to 4.1%. With larger admixtures of

$\text{H}_2\text{O}$ , a larger fraction of the energy deposition is through vibrational and rotational excitation of  $\text{H}_2\text{O}$ , resulting in less efficient dissociation of  $\text{H}_2\text{O}$ .

### C. Oxygen admixture

Addition of  $\text{O}_2$  to the He feed gas is typically performed with the goal of increasing the production of O,  $\text{O}_2^*$ , and  $\text{O}_3$ . The breakdown and IW dynamics with  $\text{O}_2$  admixtures are similar to those for an  $\text{H}_2\text{O}$  admixture. As the  $\text{O}_2$  concentration was increased from 2.4 ppm (the *as delivered impurities*) to 0.7%, the speed of the IW increased resulting in the plasma reaching the outlet of the tube 30 ns earlier. (The IW wave arrives at the end of the tube at 74 ns for 2.4 ppm.) Electron impact ionization in the IW front increased from  $1.6 \times 10^{20}\ \text{cm}^{-3}\ \text{s}^{-1}$  to  $7.5 \times 10^{20}\ \text{cm}^{-3}\ \text{s}^{-1}$ , and the electron density increased by a factor of 11 with increasing  $\text{O}_2$  admixture, indicating a more intense IW.

With adding  $\text{O}_2$  to the He flow, the electron lifetime decreased even more rapidly than for  $\text{H}_2\text{O}$  admixtures due to the more energetically favorable attachment to  $\text{O}_2$ . The thermal rate coefficient for 3-body electron attachment to  $\text{O}_2$  is  $2 \times 10^{-31}\ \text{cm}^6\ \text{s}^{-1}$ . Dissociative electron attachment to  $\text{H}_2\text{O}$  has a threshold energy of 4.3 eV. For the 0.7%  $\text{O}_2$  case,  $n_e$  in the tube decayed to  $9 \times 10^8\ \text{cm}^{-3}$  within 600 ns, whereas at this time for the base case,  $n_e = 5 \times 10^{12}\ \text{cm}^{-3}$ . The total energy deposition increased monotonically with  $\text{O}_2$  admixture, starting at  $14.7\ \mu\text{J}$  for the base case and increasing to  $127\ \mu\text{J}$  for 0.7%  $\text{O}_2$ . As the mole fraction of  $\text{O}_2$  increased, the electron density increased from  $3 \times 10^{12}$  to  $9 \times 10^{12}\ \text{cm}^{-3}$ , while  $T_e$  remained similar in the IW front ( $T_e \approx 5.8\ \text{eV}$ ) but was elevated for a shorter time (lower  $T_e$  in the bulk plasma). The rate of energy loss by electrons after the initial IW propagation was more rapid for larger  $\text{O}_2$  mole fractions due to the higher rate of energy loss collisions with the molecular additive.

The energy deposition and volume integrated number densities (or inventories) of RONS as a function of  $\text{O}_2$  admixture at  $1\ \mu\text{s}$  after the voltage pulse are shown in Fig. 9. The energy deposition initially increases with the  $\text{O}_2$  admixture as Penning ionization increases and the ionization rate, electron density, and conductivity increase. At larger admixtures, electron attachment to  $\text{O}_2$  begins to reduce this conductivity and limit further increases in energy deposition. The species with initial inventories which increased with  $\text{O}_2$  admixture include  $\text{O}_2^*$ ,  $\text{O}_2^{**}$ , O,  $\text{O}_3$ , and  $\text{N}_2(\text{v})$ . The production of  $\text{O}_2^*$  and  $\text{O}_2^{**}$  was a direct result of the increase in electron impact collisions with  $\text{O}_2$ . The production of O increased as a result of increasing electron densities, with  $\text{O}_2^+$  being the dominant ion leading to O formation by  $e + \text{O}_2^+ \rightarrow \text{O} + \text{O}$ . The inventory of  $\text{O}_3$  initially increased with  $\text{O}_2$  admixture because its production is a direct consequence of O formation. The  $\text{N}_2(\text{v})$  increased due to increased energy deposition and further propagation of the faster IW outside of the tube. A few species have inventories which decreased monotonically with  $\text{O}_2$  admixture, including H,  $\text{H}_2$ , N, and  $\text{N}^*$ . As more  $\text{O}_2$  was added,  $\text{H}_2\text{O}^+$  and  $\text{N}_2^+$  charge exchanged with  $\text{O}_2$ , which prevented these ions from undergoing the dissociative recombination reactions which are a dominant

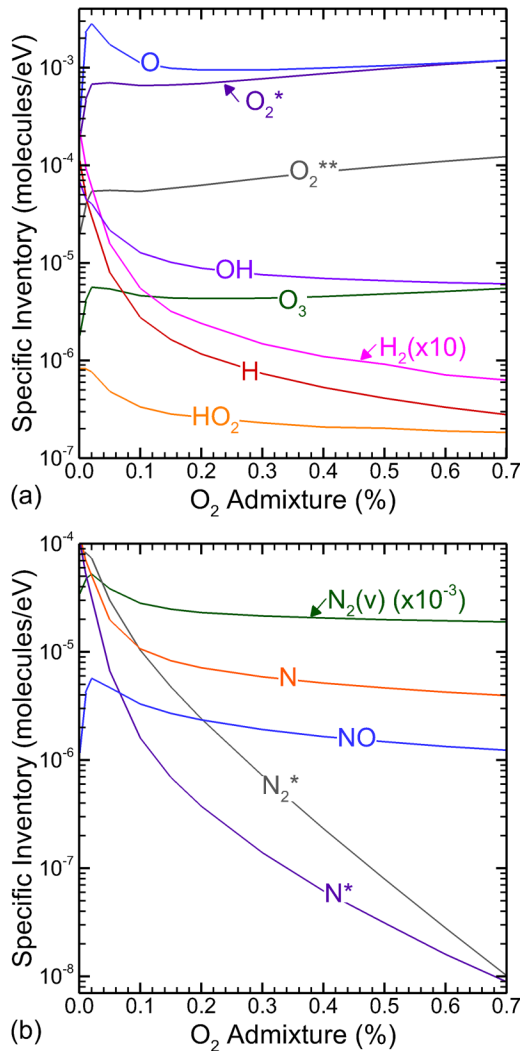


FIG. 10. The inventories of ROS and RNS at 1  $\mu$ s after the start of the voltage pulse per eV of energy deposition in the plasma (the specific inventory) as a function of O<sub>2</sub> admixture. (a) ROS and (b) RNS.

source of N, N\*, and H:  $e + N_2^+ \rightarrow N + N^*$  and  $e + H_2O^+ \rightarrow OH + H$ .

The other species with significant densities at this time, OH, NO, HO<sub>2</sub>, and N<sub>2</sub>\*, have a maximum inventory at an intermediate O<sub>2</sub> admixture. At low O<sub>2</sub> admixture, OH was dominantly produced during the first  $\mu$ s inside the tube by dissociative recombination,  $e + H_2O^+ \rightarrow OH + H$ . Following this initial sourcing of OH, most of the OH production occurred later by formation of hydronium,  $H_2O^+ + H_2O \rightarrow H_3O^+ + OH$ . As the O<sub>2</sub> density increased, the production of OH inside the tube fell as H<sub>2</sub>O<sup>+</sup> charge exchanged with O<sub>2</sub> instead of undergoing dissociative recombination. The production of OH outside of the tube increased as the IW propagated more rapidly with a larger O<sub>2</sub> admixture. These effects roughly balanced at 1  $\mu$ s, and the result was a weak dependence of OH on O<sub>2</sub> admixture, with an inventory around  $6 \times 10^9$  molecules.

In the base case, NO was primarily formed outside of the tube by  $N^* + O_2 \rightarrow NO + O^*$ , as the N\* produced in the tube flowed out into the ambient. As the O<sub>2</sub> admixture increased, this reaction could also occur inside the tube,

producing NO more rapidly. However, as the admixture increased further (>0.1%), N<sub>2</sub><sup>+</sup> rapidly charge exchanged with O<sub>2</sub>, instead of undergoing dissociative recombination. As a result, the maximum inventory of NO was  $2 \times 10^9$  molecules at 0.1% O<sub>2</sub>. HO<sub>2</sub> is produced by  $H + O_2 + M \rightarrow HO_2 + M$ . Initially, the increasing O<sub>2</sub> increased the rate of this reaction and so increased the amount of HO<sub>2</sub> produced at short times. However, further increasing O<sub>2</sub> decreased the production of H, eventually limiting the early production of HO<sub>2</sub>. Initially, the N<sub>2</sub>\* density increased with O<sub>2</sub> admixture as the electron density and IW propagation outside of the tube increased. As the O<sub>2</sub> admixture further increased, the inventory of N<sub>2</sub>\* decreased because it is rapidly quenched by reactions with O<sub>2</sub>.

The inventories of species 1  $\mu$ s after the voltage pulse divided by energy deposition, the specific inventories, are shown in Fig. 10 for O<sub>2</sub> admixtures. OH, N, H, H<sub>2</sub>, N\*, and HO<sub>2</sub> have specific inventories that monotonically decreased as the O<sub>2</sub> admixture increased. The specific inventories decreased as H<sub>2</sub>O<sup>+</sup> and N<sub>2</sub><sup>+</sup> increasingly charge exchanged with O<sub>2</sub>, which prevented their dissociative recombination reactions, the source of these species. The specific inventory of HO<sub>2</sub> decreased because its formation requires H. The specific inventory of HO<sub>2</sub> is less sensitive to admixture as the increase in O<sub>2</sub> allows for faster conversion of H to HO<sub>2</sub>.

O, O<sub>2</sub>\*, O<sub>2</sub>\*\*<sup>+</sup>, O<sub>3</sub>, N<sub>2</sub>\*, N<sub>2</sub>(v), and NO have specific inventories with a more complex dependence on O<sub>2</sub> admixture. The maximum fraction of energy deposited outside of the tube, 10.2%, occurs for 0.02% O<sub>2</sub>, while the total energy deposited outside the tube increases from 0.8 to 6.5  $\mu$ J with admixture. Several species have specific inventories with a local maximum at 0.02%, including N<sub>2</sub>(v), NO, O, and O<sub>3</sub>. N<sub>2</sub>(v) is dominantly produced outside the tube, and so its specific inventory correlates with the fraction of energy deposition outside of the tube. As a result of this energy deposition outside of the tube, N\* is formed close to the interface between the He and air, enabling production of NO by  $N^* + O_2 \rightarrow NO + O^*$  to occur on these short time scales. The O inventory increases monotonically with O<sub>2</sub> admixture, but as the admixture is increased beyond 0.02%, much of the additional energy does not contribute to dissociation of O<sub>2</sub>. The rapid attachment of electrons limits the production of O by  $e + O_2^+ \rightarrow O + O$ , and instead O<sub>2</sub><sup>+</sup> is consumed by ion-ion neutralization— $O_2^+ + O_2^- \rightarrow O_2 + O_2$ . As the O<sub>2</sub> admixture increases above 0.2%, the O specific inventory increases, as the admixture results in more electron impact dissociation of O<sub>2</sub>\* (i.e., two-step dissociation). O<sub>3</sub> has a similar behavior as its precursor, O, but with a less significant peak at 0.02% O<sub>2</sub>. The conversion from O to O<sub>3</sub> occurs more slowly at lower admixtures (such as 0.02%), and so the specific inventory is low in spite of a larger inventory of O.

O<sub>2</sub>\* and O<sub>2</sub>\*\*<sup>+</sup> have specific inventories which monotonically increase with O<sub>2</sub> admixture, except for a slight decrease between 0.05% and 0.1% (less efficient). This minimum occurs as the production of these species transitions from being dominantly outside of the tube in the base case to dominantly inside the tube at higher admixtures.

N<sub>2</sub>\* is primarily produced outside of the tube and has a specific inventory that peaks at  $8 \times 10^{-5}$  molecules/eV with

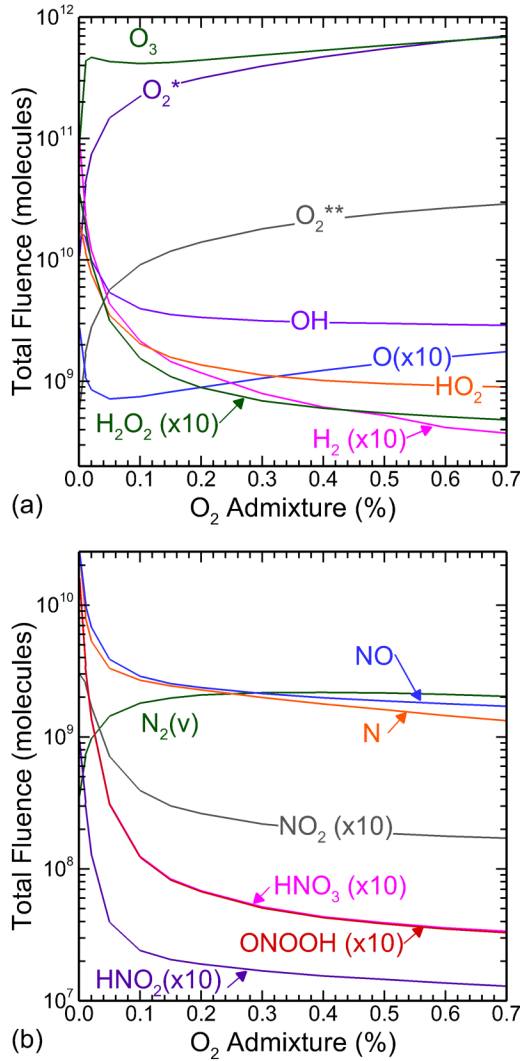


FIG. 11. The integrated fluence of RONS across the pump as a function of  $O_2$  admixture to the He flow. Despite increasing energy deposition, the fluences of many RONS decrease with increasing  $O_2$ . (a) ROS and (b) RNS.

0.01%  $O_2$ . As the  $O_2$  fraction increases, the energy deposited outside of the tube increases, but the quenching rate of  $N_2^*$  also increases, and the combination of these effects leads to the local maximum in  $N_2^*$ .

The integrated fluences of species that exit the computational domain as a function of  $O_2$  admixture are shown in Fig. 11. Only a few of these fluences increase monotonically with  $O_2$  admixture, including  $O_2^*$ ,  $O_2^{**}$ , and  $N_2(v)$ . The fluences of  $O_2^*$  and  $O_2^{**}$  increase because both  $n_e$  and the  $O_2$  density increased, and these species are a direct result of electron impact reactions.  $N_2(v)$  is primarily produced outside of the tube, and its fluence increased as the propagation of the IW outside of the tube increased.

Most RONS fluences monotonically decreased with  $O_2$  admixture, including OH,  $HO_2$ ,  $H_2$ ,  $H_2O_2$ , NO, N,  $NO_2$ ,  $HNO_3$ , ONOOH, and  $HNO_2$ . These species are produced by reactions involving OH, H, N, and  $N^*$ , which are dominantly produced by dissociative recombination of  $H_2O^+$  and  $N_2^+$ . Adding  $O_2$  results in charge exchange reactions which rapidly deplete these ion densities prior to dissociative recombination.

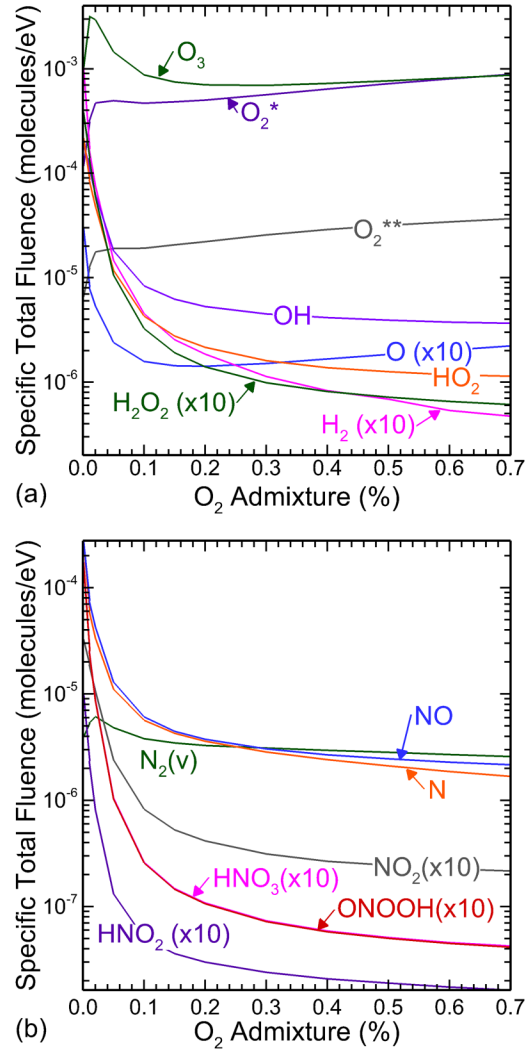


FIG. 12. The total fluence of RONS exiting through the pump per eV of energy deposition in the plasma (the specific fluence) as a function of  $O_2$  admixture to the He flow. (a) ROS and (b) RNS.

The fluences of  $O_3$  and O have a more complex behavior as a function of  $O_2$  admixture. By the time the reactive plume reaches the pump, most of the O has converted into  $O_3$ . The primary mechanism of O production at low admixtures is  $e + O_2^+ \rightarrow O + O$ . At higher  $O_2$  densities, electron impact processes dominate in producing O, in particular  $e + O_2^* \rightarrow O^* + O + e$ . As a result, the  $O_3$  fluence initially increased (due to increasing  $O_2^+$  production), reaching  $5 \times 10^{11}$  molecules, then decreases as the electron attachment to  $O_2$  occurs faster than recombination with  $O_2^+$ . At  $O_2$  mole fractions greater than 0.1%, the  $O_3$  fluence increases with admixture because of the increase in two step dissociation of  $O_2^*$ . The O fluence decreases to  $7 \times 10^7$  atoms as the admixture increases up to 0.05%  $O_2$  as a result of faster conversion to  $O_3$ . For admixtures greater than 0.05%, there is some long timescale production of O by the quenching of  $O_3$  ( $O_2^* + O_3 \rightarrow O_2 + O_2 + O$  and  $O_2^{**} + O_3 \rightarrow O_2 + O_2 + O$ ).

The total fluences divided by the energy deposition as a function of  $O_2$  admixture are shown in Fig. 12. The specific fluences of  $O_2^*$ ,  $O_2^{**}$ , OH, N, and  $N_2(v)$  follow the same trends as their specific inventories at  $1 \mu s$ , though quenching

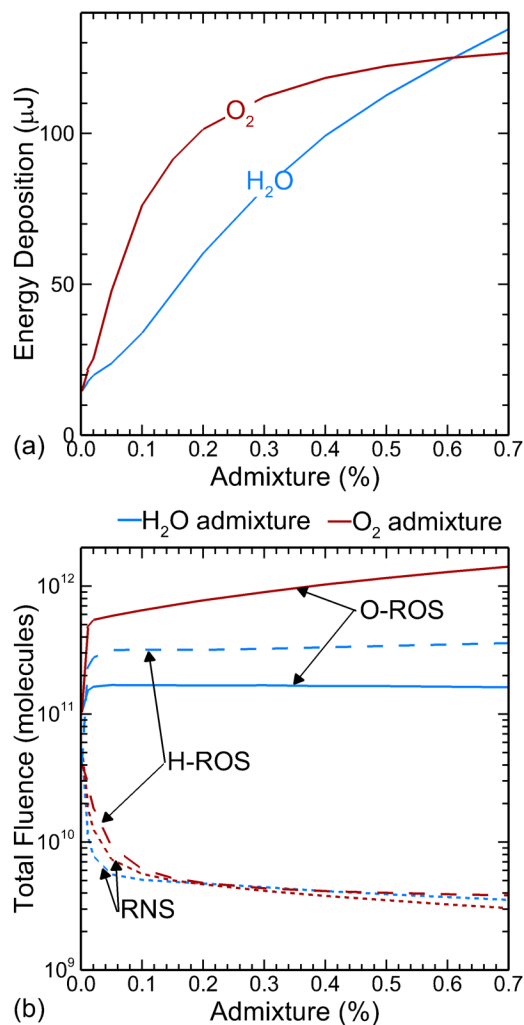


FIG. 13. Comparison of trends for H<sub>2</sub>O and O<sub>2</sub> admixtures. (a) Energy deposition. (b) Fluences of hydrogen-containing ROS (H-ROS) including the sum of OH, H<sub>2</sub>O<sub>2</sub>, and HO<sub>2</sub>, ROS which do not contain hydrogen (O-ROS) including O, O<sub>2</sub><sup>\*</sup>, O<sub>2</sub><sup>\*\*</sup>, and O<sub>3</sub>, and RNS including N, NO, NO<sub>2</sub>, HNO<sub>2</sub>, HNO<sub>3</sub>, and ONOOH.

and reactions deplete the initial inventories. N<sub>2</sub>(v) still has a local maximum at 0.02% O<sub>2</sub>, while O<sub>2</sub><sup>\*</sup> and O<sub>2</sub><sup>\*\*</sup> still generally increase with admixture, except for a slight decrease between 0.05% and 0.1% O<sub>2</sub>. The trends of the specific total fluence of O<sub>3</sub>, H<sub>2</sub>O<sub>2</sub>, H<sub>2</sub>, and HO<sub>2</sub> follow the same trends as the specific inventory of their precursors—O for O<sub>3</sub>, OH for H<sub>2</sub>O<sub>2</sub>, and H for HO<sub>2</sub> and H<sub>2</sub>. O<sub>3</sub> has a local maximum at 0.02% O<sub>2</sub>, which is consistent with the trends for O atoms at 1 μs. The specific total fluence for H<sub>2</sub>O<sub>2</sub> decreases by approximately 2 orders of magnitude as the first 0.1% O<sub>2</sub> is added, while the specific inventory of OH decreases by approximately an order of magnitude in this range. The H specific inventory decreased by more than 2 orders of magnitude as the admixture increased to 0.7%, as did the specific total fluences of HO<sub>2</sub> and H<sub>2</sub>. NO<sub>2</sub> and HNO<sub>x</sub> have specific fluences which monotonically decrease with O<sub>2</sub> admixture because they are formed from NO, and therefore, their efficiency of generation generally follow the trends for NO. The significant decrease in the specific inventory of NO is a result of rapid charge exchange from N<sub>2</sub><sup>+</sup> with O<sub>2</sub>, limiting dissociative recombination which forms

N<sup>\*</sup> and leads to NO production. The specific total fluence of NO decreases from  $3 \times 10^{-4}$  to  $2 \times 10^{-6}$  molecules/eV as the O<sub>2</sub> admixture is increased to 0.7%. The specific fluence of O has a minimum at 0.2% O<sub>2</sub>, for the reasons described above (rate of conversion to O<sub>3</sub> versus production of O by reaction of O<sub>3</sub> with O<sub>2</sub><sup>\*</sup> or O<sub>2</sub><sup>\*\*</sup>).

#### D. Comparing admixtures

The consequences of H<sub>2</sub>O and O<sub>2</sub> admixtures on RONS production are compared in Fig. 13. The total energy deposition, shown in Fig. 13(a), increases more rapidly when adding O<sub>2</sub> before leveling off around 0.5% O<sub>2</sub>. Electron attachment to O<sub>2</sub> begins to limit the electron density during the voltage pulse and therefore the energy deposition at higher admixtures. The more rapid initial rise in energy deposition with O<sub>2</sub> admixture is due to the lower power deposition in non-ionizing collisions in O<sub>2</sub> enabling a higher electron density compared to H<sub>2</sub>O. The energy deposition increases nearly linearly with H<sub>2</sub>O admixture as attachment has a relatively minor effect on the electron density on time scales of the voltage pulse. Adhikari *et al.*<sup>23</sup> observed a sharper current rise when O<sub>2</sub> or H<sub>2</sub>O was added to a He APPJ with a 1 ms voltage pulse. This observation is consistent with the increased energy deposition for the shorter voltage pulse predicted in this study.

The reactive species produced with each admixture can be grouped into RNS (N, NO, NO<sub>2</sub>, and HNO<sub>x</sub>), hydrogen containing ROS (H-ROS: OH, H<sub>2</sub>O<sub>2</sub>, and HO<sub>2</sub>), and ROS not containing hydrogen (O-ROS: O, O<sub>2</sub><sup>\*</sup>, O<sub>2</sub><sup>\*\*</sup>, and O<sub>3</sub>). H<sub>2</sub> and N<sub>2</sub>(v) have not been included in this analysis as they are less reactive and are not typically considered RONS. The sum of the total fluences of each group of species is shown in Fig. 13(b). The most abundant RNS are N and NO. The most abundant H-ROS are OH and H<sub>2</sub>O<sub>2</sub>, and the most abundant O-ROS is O<sub>3</sub>. Adding the first 0.15% of either H<sub>2</sub>O or O<sub>2</sub> decreases the RNS fluence by an order of magnitude. Any N<sub>2</sub><sup>+</sup> formed from the impurities charge exchanges with the admixture before undergoing dissociative recombination to form N<sup>\*</sup>. Above 0.15%, the RNS production is relatively insensitive to admixture. This portion of the RNS generation is primarily a result of electron impact reactions with N<sub>2</sub> inside the tube as well as production outside of the tube, rather than the dissociative recombination of N<sub>2</sub><sup>+</sup>. This behavior was observed with NO measurements by van Gessel *et al.* upon adding O<sub>2</sub> to an Ar APPJ.<sup>24</sup>

The selectivity of producing RONS with H<sub>2</sub>O compared to O<sub>2</sub> admixtures is also shown in Fig. 13(b). Adding O<sub>2</sub> increases O-ROS, but decreases H-ROS. O<sub>2</sub> has a lower ionization potential than H<sub>2</sub>O. H<sub>2</sub>O<sup>+</sup> which is formed from impurities charge exchanges with O<sub>2</sub> before undergoing dissociative recombination which disrupts the production of OH and H. Adding H<sub>2</sub>O increases both H-ROS and O-ROS. This lack of specificity is due to the production of O from H<sub>2</sub>O dissociation, and charge exchange from H<sub>2</sub>O<sup>+</sup> to O<sub>2</sub> impurities, followed by dissociative recombination of O<sub>2</sub><sup>+</sup>.

#### E. Impurities

The base case used a gas mixture based on expected impurities in ultrahigh purity helium as provided by gas

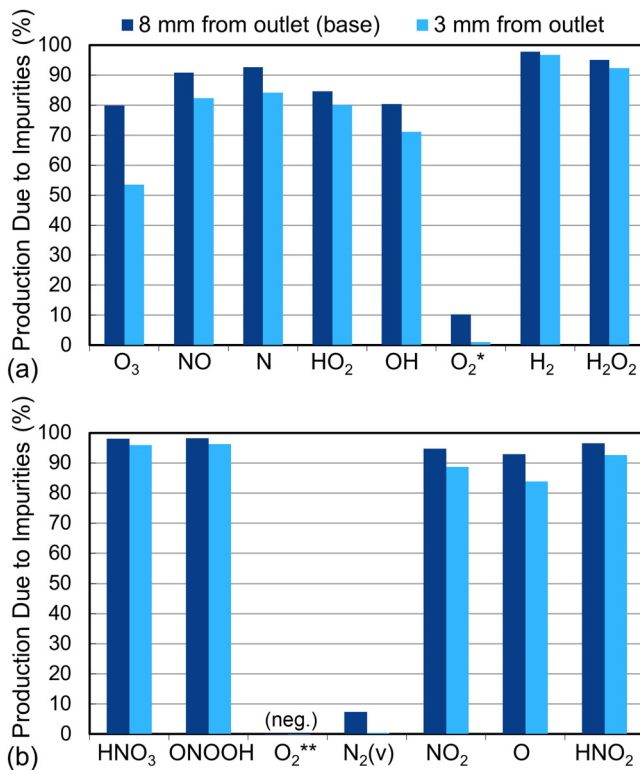


FIG. 14. Percent of the production in the base case of RONS that can be attributed to humid air impurities in the He totaling 10 ppm. These values were obtained by repeating the simulation without impurities and comparing the total fluences of RONS crossing the pump surface. Species are listed from left to right in order of decreasing total fluence. This value depends on the position of the powered electrode, with results shown here for the powered electrode being 8 mm from the outlet (the base case) and 3 mm. (a) O<sub>3</sub>, NO, N, HO<sub>2</sub>, OH, O<sub>2</sub><sup>\*</sup>, H<sub>2</sub>, and H<sub>2</sub>O<sub>2</sub>. (b) HNO<sub>3</sub>, ONOOH, O<sub>2</sub><sup>\*\*</sup>, N<sub>2</sub>(v), NO<sub>2</sub>, O, and HNO<sub>2</sub>.

suppliers. In this section, the IW and RONS generated by the base case (with impurities in the He of O<sub>2</sub>/N<sub>2</sub>/H<sub>2</sub>O = 2.4/2.9/4.7 ppm) are compared to a case that uses absolutely pure helium flowing into the tube. This comparison contrasts the ideal plasma jet with a more common plasma jet where the He is not additionally purified from its *as delivered* composition to reduce the role of these impurities. Impurities from the ambient can also certainly contaminate even absolutely pure He, but since those sources are usually system specific due to leak rates and bake-out procedures, they will not be discussed here.  $S_e$ ,  $n_e$ , and  $T_e$  during the 200 ns plasma-on period were nearly indistinguishable for the pure-He case due to the impurities being at such a low concentration. The total energy deposition in the base case with *as delivered impurities* was 14.7  $\mu$ J and 14.2  $\mu$ J without impurities. During the afterglow, the electron density had a slightly faster decay rate in the base case because of the possibility of attachment reactions inside the tube.

The cascade of charge exchange and dissociative recombination that occurred inside the tube in the base case, producing much of the RONS, does not occur in the absence of impurities. Without impurities, the dominant positive ion was He<sub>2</sub><sup>+</sup> and the dominant negative species was electrons well into the afterglow. In contrast, by 5  $\mu$ s into the afterglow in the base case, the dominant positive ion was O<sub>2</sub><sup>+</sup>. The fluences of

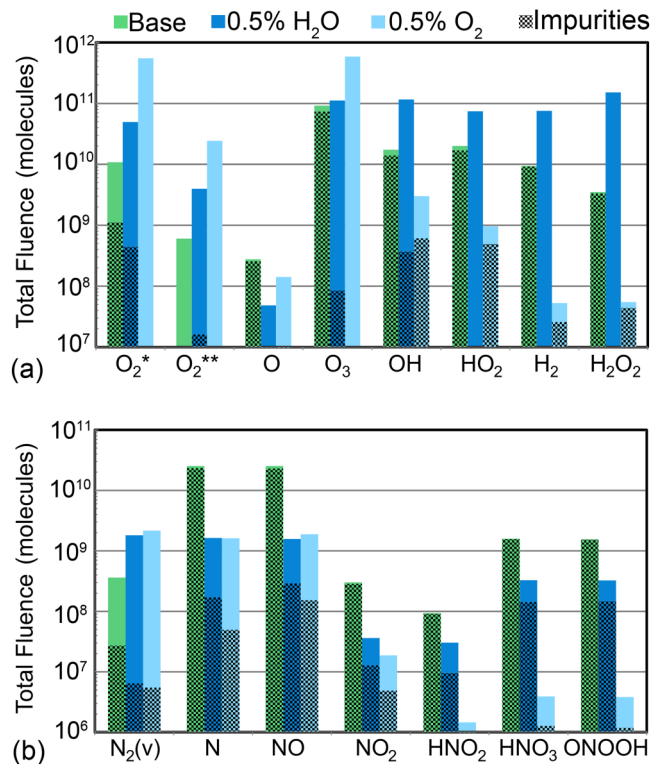


FIG. 15. Total fluence of RONS for the base case, a 0.5% H<sub>2</sub>O admixture, and a 0.5% O<sub>2</sub> admixture. The amount of each species fluence can be attributed to humid air impurities in the He totaling 10 ppm is shaded. (a) ROS and (b) RNS.

RONS which were collected at the pump were significantly influenced by the impurities. The differences in the fluences of RONS generated by the base case compared to the ideal case can be attributed to the impurities. These differences are shown as a percent of the total generation of the base case in Fig. 14. These values were calculated by running one simulation with impurities (the base case) and one with absolutely pure helium and calculating the percent difference in the total integrated fluences collected at the pump. For nearly all species, the impurities were responsible for more than 70% of the generation of the RONS. The exceptions are O<sub>2</sub><sup>\*</sup>, O<sub>2</sub><sup>\*\*</sup>, and N<sub>2</sub>(v). O<sub>2</sub><sup>\*\*</sup> actually showed an increase in its fluence in the case of absolutely pure He. In the base case, these species were mainly produced outside of the tube during the plasma-on period, so they were relatively insensitive to impurities.

These results are highly sensitive to the time and length of propagation of the IW in the ambient compared to the time of propagation in the tube. For example, moving the powered electrode closer to the end of the tube (from 8 mm to 3 mm) results in the IW propagating further into the ambient. The IW extends 4 mm from the end of the tube when the powered electrode is moved closer to the end of the tube, compared to 3 mm in the base case. The energy deposited outside of the tube increases from 0.8 to 5.1  $\mu$ J.<sup>22</sup> This change in the IW propagation leads to greater RONS production and more of the reactivity being generated outside of the tube. The sensitivity of RONS production to the impurities in the He flow is up to 26% lower than for the base case, as shown in Fig. 14. This is in part because more RONS are

produced in the 3 mm case than the base case, and so the contributions of the impurities are smaller fractions of the total RONS.

Including an intentional molecular admixture also reduces the consequences of the impurities on RONS production, as shown in Fig. 15. The production due to impurities was calculated by repeating the simulations without the 10 ppm impurities in the He flow in the case of 0.5% H<sub>2</sub>O and 0.5% O<sub>2</sub>. The concentration of admixture, however, was kept constant even when removing impurities. For example, when the 0.5% H<sub>2</sub>O case was repeated without impurities, only the N<sub>2</sub> and O<sub>2</sub> flowing into the tube were removed, and the H<sub>2</sub>O mole fraction was unchanged. The total fluence at the pump was then subtracted from the case containing impurities to yield the production due to impurities, which is shaded in Fig. 15. Both admixtures significantly reduce the fraction of RONS production that is a result of impurities.

With an H<sub>2</sub>O admixture, the production of species which originate from H<sub>2</sub>O dissociation (OH, HO<sub>2</sub>, H<sub>2</sub>, and H<sub>2</sub>O<sub>2</sub>) are independent of having impurities because the H<sub>2</sub>O density is essentially the same with and without impurities. O<sub>3</sub> production is also nearly independent of impurities with an H<sub>2</sub>O admixture (impurities contribute <0.1%) because the production of O, its precursor, occurs inside the tube primarily by  $e + H_2O^+ \rightarrow O + H + H$ . The production of excited states [O<sub>2</sub><sup>\*</sup>, O<sub>2</sub><sup>\*\*</sup>, N<sub>2</sub>(v)] tends to be much less dependent on impurities because they are primarily generated outside of the tube. 10%-45% of the production of nitrogen containing species is still a result of the N<sub>2</sub> impurities in the He even with H<sub>2</sub>O admixtures. Though the fraction of production due to impurities remains above 10% for RNS, the total of amount of RNS produced is also reduced by the addition of an admixture. Therefore, the production of, for example, NO by impurities decreases from  $2 \times 10^{10}$  molecules for the base case to  $3 \times 10^8$  molecules when an H<sub>2</sub>O admixture is present. The decrease in the contribution of impurities to RNS production with admixtures results from charge exchange depleting the N<sub>2</sub><sup>+</sup> before dissociative recombination can produce the N and N\* precursors. The energy deposition outside of the tube is also larger, so more RNS are produced outside the tube, where the ambient gas composition is independent of impurities.

For an O<sub>2</sub> admixture, O<sub>3</sub> and O production are not dependent on impurities, because they are a result of dissociation of O<sub>2</sub> in the tube, which does not change based on the H<sub>2</sub>O or N<sub>2</sub> impurities. The species which require the dissociation of H<sub>2</sub>O (OH, HO<sub>2</sub>, H<sub>2</sub>, and H<sub>2</sub>O<sub>2</sub>) attribute 20%-80% of their production to impurities, with a significant portion of the H<sub>2</sub>O dissociation occurring inside the tube. The RNS generation is less dependent on the impurities with an O<sub>2</sub> admixture (3%-32%) than a H<sub>2</sub>O admixture. In addition to the charge exchange that depletes N<sub>2</sub><sup>+</sup> densities, rapid electron attachment occurs in the presence of O<sub>2</sub>. N<sub>2</sub><sup>+</sup> is more likely to undergo ion-ion recombination (O<sub>2</sub><sup>-</sup> + N<sub>2</sub><sup>+</sup> → O<sub>2</sub> + N<sub>2</sub>) rather than the dissociative recombination which facilitates NO formation ( $e + N_2^+ \rightarrow e + N + N^*$ ). As a result, an O<sub>2</sub> admixture makes the RNS production even less sensitive to impurities than an H<sub>2</sub>O admixture.

These results indicate that an admixture can be used to improve the control and consistency of the chemistry generated

by an APPJ, rather than having reactive species production depend on the impurities in the gas supply which may not be well controlled or well known.

#### IV. CONCLUDING REMARKS

This computational investigation has shown that the addition of a molecular admixture to a He atmospheric pressure plasma jet can have a significant impact on the ionization wave propagation speed, electron density, electron temperature, initial RONS production, and the final chemistry which is delivered in the effluent. In the base case, which contained *as delivered impurities* in the helium, most of the dissociation occurred in the cascade of charge exchange and dissociative recombination in the afterglow, rather than during the discharge pulse. At constant voltage, adding an H<sub>2</sub>O or O<sub>2</sub> admixture as high as 0.7% increased the energy deposition and the IW speed. The majority of the effects on the chemistry were achieved within the first 0.1% of admixture, above which changes in composition began to saturate.

For H<sub>2</sub>O admixtures, rapid charge exchange depleted the density of N<sub>2</sub><sup>+</sup> resulting from the base *as delivered impurities*, decreasing the production of N\*, and therefore the production of NO and all other RNS. H<sub>2</sub>O<sub>2</sub>, OH, H<sub>2</sub>, and HO<sub>2</sub> fluences increased as these species are all a result of chemistry originating from H<sub>2</sub>O dissociation. The production of O<sub>3</sub> and O generally increased but had a more complex dependence as the mechanism of production shifted from dissociative recombination of O<sub>2</sub><sup>+</sup> to that of H<sub>2</sub>O<sup>+</sup>. The production efficiency of H<sub>2</sub>O<sub>2</sub>, OH, H<sub>2</sub>, and HO<sub>2</sub> reach their maxima between 0.01% and 0.05% H<sub>2</sub>O. Adding H<sub>2</sub>O beyond this value significantly increased the energy deposition, while only slightly increasing the production of these species.

O<sub>2</sub> admixtures decreased the fluences of all RNS and the species which require the dissociation of H<sub>2</sub>O. Significant O<sub>2</sub> in the He flow resulted in rapid charge exchange to consume N<sub>2</sub><sup>+</sup> and H<sub>2</sub>O<sup>+</sup>, which would otherwise undergo dissociative recombination. O fluences had a local minimum at 0.05% O<sub>2</sub>. Below this value, O reached the pump face prior to reacting with O<sub>2</sub> to form O<sub>3</sub>. Above this value, the slow quenching of O<sub>3</sub> by O<sub>2</sub><sup>\*</sup> and O<sub>2</sub><sup>\*\*</sup> generated significant amounts of O downstream. The O<sub>3</sub> fluence had a non-monotonic dependence on admixture because the primary production pathway for O atoms changed from dissociative recombination of O<sub>2</sub><sup>+</sup> at low admixture to electron impact dissociation of O<sub>2</sub><sup>\*</sup> at large admixture. The production efficiency of species that require the dissociation of H<sub>2</sub>O or N<sub>2</sub> decreased monotonically as the O<sub>2</sub> admixture increased. The O<sub>3</sub> production efficiency was maximum at 0.01% O<sub>2</sub>, while the energy efficiency of O<sub>2</sub><sup>\*</sup> and O<sub>2</sub><sup>\*\*</sup> generally increased with admixture.

Without intentional admixtures, manufacturer stated impurities accounted for 79%-98% of the O<sub>3</sub>, NO, N, HO<sub>2</sub>, OH, H<sub>2</sub>, H<sub>2</sub>O<sub>2</sub>, HNO<sub>3</sub>, ONOOH, NO<sub>2</sub>, O and HNO<sub>2</sub> fluences which reach the pump. APPJs having a larger energy deposition outside of the tube or using O<sub>2</sub> or H<sub>2</sub>O admixtures reduces the sensitivity of RONS generation to impurities at the ppm level and may provide better control of that generation.

The addition of O<sub>2</sub>, because it has a lower ionization energy than N<sub>2</sub> or H<sub>2</sub>O, provides more selectivity as it only increases the production of O, O<sub>3</sub>, O<sub>2</sub><sup>\*</sup>, and O<sub>2</sub><sup>\*\*</sup> and decreases the production of RNS and hydrogen-containing ROS (OH, H<sub>2</sub>O<sub>2</sub>, HO<sub>2</sub>). The trade-off is that the production of hydrogen-containing ROS, while lower, is still sensitive to impurities at the ppm level (which are often uncontrolled). H<sub>2</sub>O admixtures demonstrate less selectivity in RONS production as increasing the H<sub>2</sub>O mole fraction tends to increase the production of all ROS. This decreased selectivity has the advantage of making the production of all of the ROS nearly independent of impurities in the helium.

## ACKNOWLEDGMENTS

This work was supported by the Department of Energy Office of Fusion Energy Science (Nos. DE-SC000319 and DE-SC0014132), the National Science Foundation (NSF) (No. PHY-1519117), and the NSF Graduate Research Fellowship Program.

<sup>1</sup>Z.-H. Lin, C.-Y. Tobias Tschang, K.-C. Liao, C.-F. Su, J.-S. Wu, and M.-T. Ho, *IEEE Trans. Plasma Sci.* **44**, 3140 (2016).

<sup>2</sup>I. Adamovich *et al.*, *J. Phys. D Appl. Phys.* **50**, 323001 (2017).

<sup>3</sup>J. Schlegel, J. Körtzer, and V. Boxhammer, *Clin. Plasma Med.* **1**, 2 (2013).

<sup>4</sup>M. Ito, T. Ohta, and M. Hori, *J. Korean Phys. Soc.* **60**, 937 (2012).

<sup>5</sup>G.-M. Xu, X.-M. Shi, J.-F. Cai, S.-L. Chen, P. Li, C.-W. Yao, Z.-S. Chang, and G.-J. Zhang, *Wound Repair Regen.* **23**, 878 (2015).

<sup>6</sup>S. Bekeschus, K. Wende, M. M. Hefny, K. Rödder, H. Jablonowski, A. Schmidt, T. von Woedtke, K.-D. Weltmann, and J. Benedikt, *Sci. Rep.* **7**, 2791 (2017).

<sup>7</sup>G. Isbary *et al.*, *Clin. Plasma Med.* **1**, 25 (2013).

<sup>8</sup>D. Dobrin, M. Magureanu, N. B. Mandache, and M. D. Ionita, *Innov. Food Sci. Emerg. Technol.* **29**, 255 (2015).

<sup>9</sup>G. Bauer and D. B. Graves, *Plasma Process. Polym.* **13**, 1157 (2016).

<sup>10</sup>D. B. Graves, *Clin. Plasma Med.* **2**, 38 (2014).

<sup>11</sup>X. Lu, M. Laroussi, and V. Puech, *Plasma Sources Sci. Technol.* **21**, 034005 (2012).

<sup>12</sup>P. Bruggeman, F. Iza, D. Lauwers, and Y. A. Gonzalvo, *J. Phys. D Appl. Phys.* **43**, 12003 (2010).

<sup>13</sup>T. Verreycken, R. Mensink, R. van der Horst, N. Sadeghi, and P. J. Bruggeman, *Plasma Sources Sci. Technol.* **22**, 055014 (2013).

<sup>14</sup>N. Knake, S. Reuter, K. Niemi, V. Schulz-von der Gathen, and J. Winter, *J. Phys. D Appl. Phys.* **41**, 194006 (2008).

<sup>15</sup>G. V. Naidis, *Plasma Sources Sci. Technol.* **23**, 065014 (2014).

<sup>16</sup>G. Park, H. Lee, G. Kim, and J. K. Lee, *Plasma Process. Polym.* **5**, 569 (2008).

<sup>17</sup>S. Schröter, A. R. Gibson, M. J. Kushner, T. Gans, and D. O'Connell, *Plasma Phys. Control. Fusion* **60**, 014035 (2018).

<sup>18</sup>H. M. Joh, J. Y. Choi, S. J. Kim, T. H. Chung, and T.-H. Kang, *Sci. Rep.* **4**, 6638 (2014).

<sup>19</sup>S. A. Norberg, E. Johnsen, and M. J. Kushner, *Plasma Sources Sci. Technol.* **24**, 035026 (2015).

<sup>20</sup>S. Norberg, "Modeling atmospheric pressure plasma jets: Plasma dynamics, interaction with dielectric surfaces, liquid layers and cells," Ph.D. thesis (University of Michigan, 2015), see <http://hdl.handle.net/2027.42/113342>

<sup>21</sup>D. X. Liu, P. Bruggeman, F. Iza, M. Z. Rong, and M. G. Kong, *Plasma Sources Sci. Technol.* **19**, 025018 (2010).

<sup>22</sup>A. M. Lietz and M. J. Kushner, "Electrode configurations in atmospheric pressure plasma jets: Production of reactive species," *Plasma Sources Sci. Technol.* (published online).

<sup>23</sup>E. R. Adhikari, V. Samara, and S. Ptasinska, *J. Phys. D* **51**, 185202 (2018).

<sup>24</sup>A. F. H. van Gessel, K. M. J. Alards, and P. J. Bruggeman, *J. Phys. D Appl. Phys.* **46**, 265202 (2013).